International Journal of Pharmaceutics 416 (2011) 210–222

Contents lists available at ScienceDirect

International Journal of Pharmaceutics

journal homepage: www.elsevier.com/locate/ijpharm

A comparison of ram extrusion by single-holed and multi-holed dies for extrusion–spheronisation of microcrystalline-based pastes

M. Zhang[a], S.L. Rough[a], R. Ward[b], C. Seiler[b], D.I. Wilson[a,*]

[a] Department of Chemical Engineering and Biotechnology, New Museums Site, Pembroke Street, Cambridge CB2 3RA, UK
[b] MSD, Hertford Road, Hoddesdon, Hertfordshire EN11 9BU, UK

ARTICLE INFO

Article history:
Received 15 April 2011
Received in revised form 20 June 2011
Accepted 24 June 2011
Available online 30 June 2011

Keywords:
Extrusion–spheronisation
Microcrystalline cellulose
Multi-holed dies
Screen extrusion

ABSTRACT

The use of multi-holed dies as an alternative to single-holed dies for generating extrudates for spheronisation was investigated both in terms of extrusion and spheronisation performance. A model 45 wt% microcrystalline cellulose (MCC)/water paste was employed in ram extrusion tests with square-ended dies with 1, 6, 33 and 137 holes, all of diameter 1 mm and length 2 mm. The extrudates generated using the multi-holed dies yielded pellets with comparable sphericity to those using the single-holed die. Multi-holed dies could also be operated with lower paste flow rates before encountering liquid phase migration (LPM). The characteristic processing velocity for the onset of LPM was determined for each die configuration and supported the hypothesis that LPM was caused by suction effects. A simple model of the flow pattern in a lab-scale Fuji-Paudal frontal screen extruder is presented which yields estimates of velocities and shear rates involved in these devices. The pressure required to extrude the paste through multi-holed dies was compared with the model proposed by Benbow and co-workers. The paste rheology was characterised using the Benbow–Bridgwater approach, employing 1, 2 and 3 mm diameter dies of various lengths. The Benbow et al. model under-predicted the observed extrusion pressure, which was attributed to its failure to account for the redundant work contribution in these complex flows.

1. Introduction

Extrusion–spheronisation (E–S) is widely used in the pharmaceutical and other sectors for manufacturing dense granules with controlled, high sphericity. The particulate solids are combined with a liquid (the binder) to yield a dense suspension or paste which is extruded through dies or screens to give cylindrical extrudates. These extrudates are then spheronised (or *marumerised*) on a rotating friction plate to produce granules (Wilson and Rough, 2007). Industrial extrusion devices frequently employ screens – thin metal sheets containing many holes – in order to maximise throughput and avoid the use of high extrusion pressures, with a range of configurations including basket, cylinder and wiping configurations. These are characterised by a high fraction of the screen's surface area being occupied by holes, typically up to 25%.

Laboratory studies of extrusion–spheronisation, however, often employ relatively small volumes of sample which are ram extruded through concentric, cylindrical, single-holed dies to generate extrudates prior to spheronisation. The apparatus geometry is that of a capillary rheometer (*e.g.* Rough et al., 2000): an advantage of this configuration is that it aids analysis of the flow behaviour of the paste, such as using the characterisation procedure described by Benbow and Bridgwater (1993). It does, however, introduce two complicating aspects when applying the results to pilot and production scale machines. The first is that of simulation, in mapping the results obtained from a single-holed die to a multi-holed screen configuration. The second concerns operating velocity: the large die area provided by multi-holed dies means that the paste is fed towards the screen at a relatively low velocity, and replicating these velocities in a single-holed capillary test can lead to liquid phase migration (LPM). Ram extrusion at low velocity exposes the paste to high stresses for extended periods, and LPM arises when the stress on the liquid phase causes it to move faster than the solid phase. Over time the paste loses liquid and becomes harder to extrude as well as producing inhomogeneous extrudates, which yield poor quality spheronised product in terms of shape and size distribution (Boutell et al., 2002).

This paper explores the potential for the use of ram extrusion to characterise and assess paste formulations for screen extrusion. A single microcrystalline cellulose (MCC)/water formulation is used as the test material, being representative of many E–S formulations. Firstly, the spheronisation performance of extrudates generated by multi-holed testing is compared with single-holed routes. Multi-holed dies are shown to give comparable performance to single-holed testing, and the flow behaviour of these systems is then investigated in greater detail. Secondly, the rheological

* Corresponding author. Tel.: +44 1223 334 791; fax: +44 1223 334 796.
E-mail address: diw11@cam.ac.uk (D.I. Wilson).

0378-5173/$ – see front matter © 2011 Elsevier B.V. All rights reserved.
doi:10.1016/j.ijpharm.2011.06.043

Nomenclature

Roman

A	cross-sectional area of die hole, m^2
AR	aspect ratio
A_0	cross-sectional area of barrel, m^2
CoV	coefficient of variation
d_{CE}	circle equivalent diameter, m
d	screen hole diameter, m
D	die diameter, m
D_{ram}	ram diameter, m
D_0	barrel diameter, m
f	area fraction of screen (or die) occupied by holes
F	measured ram force, N
h_1	height at entry of nip region, m
h_2	height at exit of nip region (nip gap), m
L	die length, m
l	blade breadth, m
L_{max}, L_{min}	pellet size (maximum length, length normal to this), m
m	die entry flow index (Eq. (5))
n	die land slip velocity index (Eq. (5))
N	number of holes in die plate
p	pitch between successive rows of holes in screen, m
P_{ex}	extrusion pressure, Pa
$P_{ex,BB}$	extrusion pressure predicted by Benbow et al. model, Pa
$P_{redundant}$	redundant work per unit volume, Pa
$P_{ex,\ 25\,mm}$	extrusion pressure at a ram displacement of 25 mm, Pa
P_1	pressure drop across die entry region, Pa
P_2	pressure drop along die land, Pa
Q	volumetric flow rate, $m^3\ s^{-1}$
Q_N	volumetric flow rate through the screen per unit depth, $m^2\ s^{-1}$
r	radial co-ordinate, m
r_i	inner radius of blade, m
r_o	outer radius of blade, m
R^2	coefficient of determination
V	plug flow extrusion velocity, $m\ s^{-1}$
V_N	velocity of paste passing through a screen hole, $m\ s^{-1}$
$V_{ram,LPM}$	threshold ram velocity for LPM, $m\ s^{-1}$
V_S	screen linear velocity, $m\ s^{-1}$
V^*	superficial velocity of paste, $m\ s^{-1}$
x	length of screen active zone, m
z	axial co-ordinate, m

Greek

α	die entry velocity factor (Eq. (5)), $MPa\,(s/m)^{-m}$
β	die land (slip) velocity factor (Eq. (5)), $MPa\,(s/m)^{-n}$
$\dot{\varepsilon}$	extensional strain rate (Eq. (9)), s^{-1}
$\dot{\gamma}$	shear strain rate, s^{-1}
λ	characteristic length scale (Eq. (9)), m
σ_0	zero velocity bulk yield stress (Eq. (5)), Pa
σ_y	bulk yield stress (Eq. (4)), Pa
τ_0	zero velocity wall shear stress (Eq. (5)), Pa
τ_w	wall shear stress (Eq. (4)), Pa
ω	blade rotation speed, $rad\ s^{-1}$

behaviour of the paste is established using the Benbow–Bridgwater approach. Its extrusion behaviour through multi-holed dies is studied, and the mechanical data compared with the model proposed by Benbow et al. (1991). The multi-holed dies used (featuring small die land lengths and hole area fractions approaching 0.25) aim to represent the geometry of a screen extruder. Finally, it will be shown that LPM occurs in multi-holed dies, as in single-holed dies, but at different processing velocities. The use of multi-holed dies is investigated as a route to eliminating LPM from testing.

1.1. Screen extrusion: an approximate analysis

The timescales and extrusion velocities involved in screen extrusion can be estimated for some simple geometries. Consider the configuration in Fig. 1, which is based on a Fuji-Paudal MG-55 operating in frontal extrusion mode. The geometry of the blade and velocities were taken from a pilot plant device. A screw feeds material forward into the space vacated by the blade, where it is forced through the screen holes by the action of the rotating wiping blade. Compaction of the material is likely to occur on being subjected to the stresses associated with extrusion: such changes in density are ignored in this analysis. At steady state the material feed rate will match that passing through the screen.

Fig. 1(d) presents a side view of the blade and screen at some radius r. In the frame of reference where the blade is static, the screen moves towards the blade with linear velocity $V_S = r\omega$, where ω is now the rotational speed of the screen. The screen drags a mass of material towards a region termed the 'nip' gap (of height h_2), and we assume that there is a linear velocity profile across AD, giving the volumetric flow rate per unit depth (into the page) into the nip region ABCD as $1/2\ h_1 V_S$. This estimate is subject to considerable uncertainty as there is likely to be slip of the material at the wall and a non-uniform flow field across AD: for the purposes of this analysis, however, it sets an upper bound on the flow rate. The material entering the nip region either leaves through the nip gap or through the screen. Assuming a linear velocity profile across the nip gap gives a volumetric flow rate out of the nip per unit depth as $1/2\ h_2 V_S$. The nip gap is not fixed in screen devices, as the screen often flexes at the passing of the blade (see Baert and Down, 1994). h_2 is therefore determined by the stresses developed during extrusion and the thickness of the screen: h_2 cannot be determined *a priori*, so a set gap of 1 mm is used here. The flow rate through the screen per unit depth, Q_N, is determined by difference (assuming conservation of volume) as

$$Q_N = \frac{1}{2}h_1 V_S - \frac{1}{2}h_2 V_S = \frac{1}{2}r\omega(h_1 - h_2) \tag{1}$$

Further assumptions are required to estimate the velocity at which the material moves through the screen holes. We choose here to assume that the active zone for extrusion, length x (located at C) is $2p$, where p is the pitch between successive rows of screen holes. This is based on observations that extrudate emerges from a zone close to the blade in such devices, and this value yields an upper limit for the velocity. Other active zone sizes could be used, such as more rows of holes, without loss of generality. The area available for extrusion per unit depth is xf, where f is the area fraction of the screen occupied by holes. Assuming uniform plug flow of material at velocity V_N through each hole gives

$$V_N = \frac{Q_N}{xf} = \frac{r\omega(h_1 - h_2)}{2xf} \tag{2}$$

The dimensions and range of operating velocities for the Fuji-Paudal device are presented in Table 1. The associated range of blade velocities at the inner and outer radii of the blade are presented in Table 2, alongside the estimated extrusion velocities and apparent shear strain rates in the nip gap and the screen holes. Also given in Table 2 is the superficial velocity of the paste as it

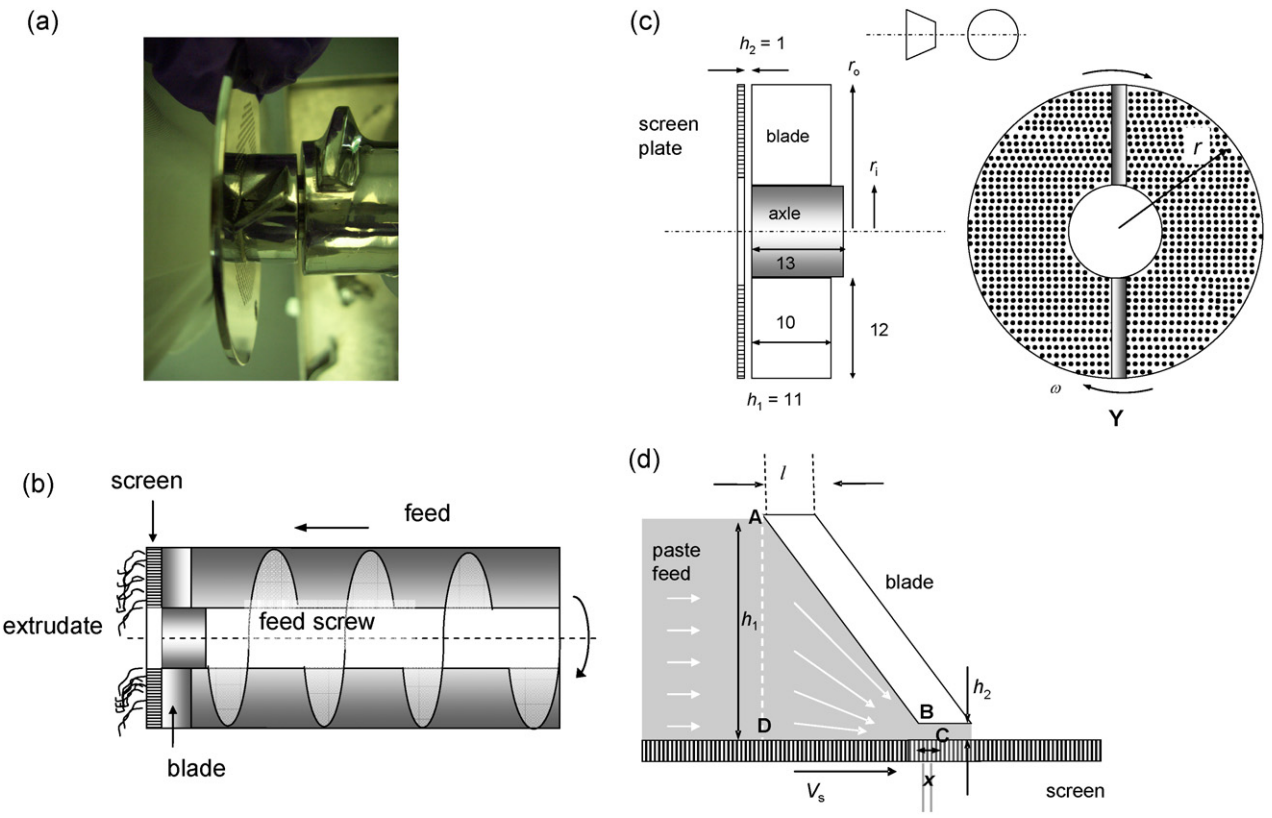

Fig. 1. Analysis of screen extruder based on Fuji-Paudal MG-55 frontal extrusion device: (a) photograph of internals and end plate (side view); (b) schematic of operation; (c) geometry of end screen and blades; (d) side view from point Y of blade and screen at radius $r_i \le r \le r_o$. Not to scale: dimensions shown in mm.

Table 1
Geometry parameters and rotational speeds estimated for Fuji-Paudal MG-55 frontal extruder.

Blade geometry	
Blade height, h_1	10 mm
Blade breadth, l	1.9 mm
Inner radius, r_i	15 mm
Outer radius, r_o	27 mm
Notional nip gap, h_2	1.0 mm
Screen holes	
Diameter, d	1.0 mm
Average pitch, p	1.8 mm
Area fraction, f	0.25
Blade rotational speed	
Lowest	1.0 rad s^{-1}
Highest	9.4 rad s^{-1}

approaches the extrusion head, V^*, given by

$$V* = \frac{Q}{\pi(r_o^2 - r_i^2)} = \frac{1}{\pi(r_o^2 - r_i^2)} \int_{r_i}^{r_o} Q_N dr = \frac{\omega(h_1 - h_2)}{2\pi(r_o^2 - r_i^2)} \int_{r_i}^{r_o} r dr$$

$$= \frac{\omega}{4\pi}(h_1 - h_2) \quad (3)$$

where Q is the volumetric flow rate of the paste feed.

The values of velocity and shear strain rates obtained from this first order model cover several orders of magnitude. The shear strain rates in the nip gap are decades smaller than those estimated for flow in a screen hole. When the rheology of the paste is sensitive to shear strain rate, this difference in rates will have a significant impact on the flow patterns and forces generated in the nip region and the screen. Since many pastes exhibit visco-plastic behaviour (and are shear-thinning), this is likely to be the case and requires

Table 2
Estimated screen extrusion parameters and paste shear strain rates in Fuji-Paudal MG-55 frontal extruder.

		Rotational speed	
		$\omega = 1.0$ rad s^{-1}	$\omega = 9.4$ rad s^{-1}
Blade speed	V_S at r_i	15 mm s^{-1}	141 mm s^{-1}
	V_S at r_o	27 mm s^{-1}	254 mm s^{-1}
Shear strain rate in nip gap[a]	$\dot{\gamma}$ at r_i	15 s^{-1}	141 s^{-1}
	$\dot{\gamma}$ at r_o	27 s^{-1}	254 s^{-1}
Extrusion velocities and flow rates	V_N at r_i	76 mm s^{-1}	720 mm s^{-1}
(From Eq. (2))	V_N at r_o	137 mm s^{-1}	1290 mm s^{-1}
	Q	1134 mm^3 s^{-1}	10 660 mm^3 s^{-1}
(From Eq. (3))	V^*	0.7 mm s^{-1}	6.7 mm s^{-1}
Apparent shear strain rate in screen hole[b]	$\dot{\gamma}$ at r_i	608 s^{-1}	5760 s^{-1}
	$\dot{\gamma}$ at r_o	1096 s^{-1}	10 300 s^{-1}

[a] Estimated from $\dot{\gamma} = V_S/h_2$.
[b] Estimated from $\dot{\gamma} = 8V_N/d$.

further investigation. The above analysis, however, provides upper bound estimates for velocities and therefore shear strain rates in screen extrusion.

Similarly, the magnitude of the velocity with which material passes through a hole, V_N, is decades greater than that at which it approaches the extrusion zone, V^*: phenomena such as LPM, which are associated with long processing times, are therefore prone to occur as the material is fed towards the extrusion zone, interrupting the performance of the device, rather than during the actual passage of material through the screen. LPM can, however, give rise to locally denser material which will block a screen hole rather than allow material to flow through it.

1.2. Multi-holed die extrusion

Concentric, square- or tapered entry dies are commonly used in rheological studies of paste extrusion as they present axisymmetric geometries for which the relationships between flow rate and extrusion pressure can be related to analytical solutions for constitutive model behaviour. Experimental data are interrogated to determine the most appropriate model and its associated parameters. Multi-holed dies degrade the symmetry and generate complex flow patterns which require numerically intensive simulation: for complicated dies, the flow rate through each hole can differ and this creates further challenges for simulations. Work on detailed numerical simulations of extrusion of metals through multi-holed dies has been reviewed by Sinha et al. (2009). The simulations are computationally intensive, even for rheologically simple materials, prompting Sinha et al. to present a simplified model which gave reasonable agreement with experimental data and could be used for preliminary design purposes.

Where there is uncertainty in the rheological behaviour, as often arises with pastes, exact predictions of flow behaviour are currently inaccessible. Benbow et al. (1991) proposed an approach for estimating the flow in multi-holed dies, built on their method for characterising the rheology of pastes using single-holed dies. In their characterisation approach, Benbow and Bridgwater (1993) assumed that the force required to extrude a paste through a concentric single-holed die, shown in Fig. 2, could be written as

$$P_{ex} = P_1 + P_2 = \sigma_y \ln\left[\frac{A_0}{A}\right] + 4\frac{L}{D}\tau_w \quad (4)$$

where A_0 is the cross-sectional area of the barrel, A the area of the die hole, L and D the die land length and diameter, respectively, and τ_w the shear stress on the wall of the die land. According to Eq. (4) the extrusion pressure, P_{ex}, comprises a contribution, labelled P_1, accounting for work done in the die entry region and a term, labelled P_2, accounting for flow along the die land. The latter is often associated with wall slip, while the P_1 term is written in terms of a plastic deformation with a velocity-dependent bulk yield stress, σ_y. Its form is based on a calculation of ideal work involved in an homogeneous deformation and does not consider redundant (irrecoverable) work explicitly. The work done is related to the amount of plastic strain via the $\ln(A_0/A)$ term. Its accuracy for describing the extrusion of perfect plastic materials through smooth, concentric single-holed dies was considered by Horrobin and Nedderman (1998) using detailed finite element method simulations with extensive re-meshing. Their results showed that the percentage contribution from redundant work to P_{ex} decreased as $\ln(A_0/A)$ increased. Since tests often involve single-holed capillary dies with large $\ln(A_0/A)$ values, this supports the use of Eq. (4) to characterise paste rheology.

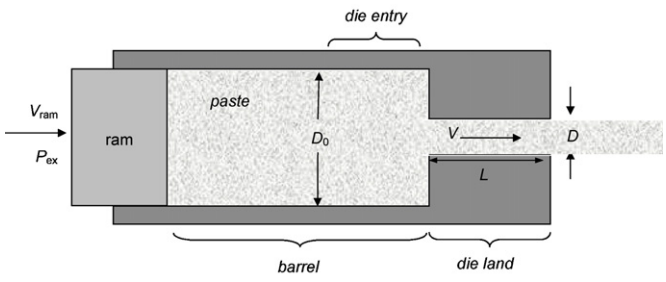

Fig. 2. Schematic of ram extrusion geometry used in paste characterisation using the Benbow and Bridgwater (1993) approach.

Where velocity (*e.g.* strain rate) effects are significant, Eq. (4) is often written in the form

$$P_{ex} = (\sigma_0 + \alpha V^m)\ln\left[\frac{A_0}{A}\right] + 4\frac{L}{D}(\tau_0 + \beta V^n) \quad (5)$$

where V is the velocity of the paste moving in plug flow along the die land, σ_0 and τ_0 are zero velocity bulk yield and wall shear stresses, and the parameters α and m, β and n describe the velocity contributions to P_1 and P_2, respectively. Benbow et al. (1991) proposed that Eq. (4) could be extended to multi-holed dies with N identical die lands by replacing the $\ln(A_0/A)$ term with one based on the sum of the die land entry areas, *viz.*

$$P_{ex} = \sigma_y \ln\left[\frac{A_0}{NA}\right] + 4\frac{L}{D}\tau_w \quad (6)$$

Rahman et al. (2001) studied the applicability of this approach for describing the extrusion of potato starch-based paste through square-entry dies with up to 6 die holes, arranged either in a ring or a ring around a central hole. They reported that Eq. (6) gave a reasonable estimate of the measured extrusion pressure, which tended to underestimate P_{ex} at higher values of N. This observation is consistent with Horrobin and Nedderman's finding that Eq. (4) would underestimate the contribution from redundant work at lower values of $\ln(A_0/A)$.

2. Materials and methods

2.1. Paste preparation

Microcrystalline cellulose (MCC, Avicel PH101) was obtained from FMC biopolymer™ (FMC corporation, Specialty Chemicals Group, Wallingstown, Little Island, Cork, Ireland). The moisture content of the MCC powder used was ~3 wt%. The MCC powder solid density was reported as 1538 kg m^{-3} (Mascia, 2008). MCC particle sizing analysis was performed using a Beckman Coulter LS230 laser diffraction instrument (Coulter Electronics Limited, Bedfordshire, UK) with deionised water as dispersant. The refractive indices of MCC and water were taken as 1.50 and 1.33, respectively (Sample dispersion and refractive index guide ©Malvern Instruments Ltd., Worcestershire, UK). The results indicated that MCC particle sizes lay in the range of 2–260 μm with a Sauter mean diameter of 49.1 μm.

45 wt% MCC/water pastes were prepared according to the following procedure. Dry MCC powder and deionised water were weighed on an electronic balance (Sartorius Mechatronics UK Ltd., Epsom, to ±0.01 g). The powder was then loaded into the bowl of a planetary mixer fitted with a 'K'-beater attachment (Kenwood Ltd., UK) and stirred at minimum speed, while water was slowly poured into the bowl. The mixture of powder and water was stirred for further periods of 2, 3, 3 and 2 min at speeds settings 1, 2, 3 and 4, respectively. Mixing was paused after each period and any caked paste dislodged from the wall of the bowl by a plastic spatula. Finally, the paste was removed from the bowl and stored in a sealed plastic sample bag at room temperature for 1 h before

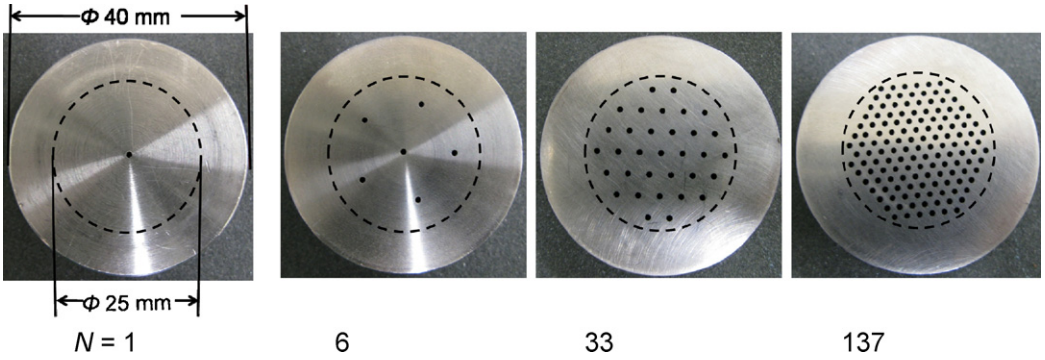

Fig. 3. Photographs of dies: stainless steel, square-entry, $D = 1$ mm, $L = 2$ mm. Dotted circles show the location of the inner wall of the barrel.

Table 3
Die hole area fractions. $D = 1$ mm, $L = 2$ mm.

Number of holes, N	Area fraction, f
1	0.0016
6	0.0096
33	0.053
137	0.22

extrusion. This allowed the water to equilibrate throughout the material.

Paste water content was determined by weighing out about 25 g paste and drying in a vacuum oven at a temperature of 60 °C and 200 mbar vacuum for 24 h. The dried sample was then weighed again to determine the mass fraction of water in the initial paste.

2.2. Extrusion–spheronisation and drying

2.2.1. Characterisation of paste rheology

Extrusion experiments were performed on 45 wt% MCC/water pastes using a 50 kN strain frame configured to operate as a ram extruder (Zwick/Roell, Zwick Testing Machines Ltd., Leominster, UK) as described by Mascia et al. (2006). The force on the ram and the ram displacement were measured using a load cell (resolution of ±0.1 N) and a displacement transducer (±1 μm), respectively. Sets of square-entry (single-holed) capillary dies with different diameters were used. The ram, barrel and dies were all made from stainless steel. A 43 mm long polyethylene seal at the end of the ram minimised paste leakage from the top of the barrel. The force due to friction between the ram and barrel was measured and found to be less than 10 N. The dimensions were: ram diameter, $D_{ram} = 24.82$ mm; barrel diameter, $D_0 = 25$ mm; die diameters, $D = 1$, 2 and 3 mm; die lengths, L, varying from 2 to 36 mm. The maximum ram velocity achievable with the strain frame was 10 mm s^{-1}. Paste samples were pre-compacted using a blank die, filling about 94 g of paste into the barrel and tamping it down by hand to an initial height of about 160 mm. The paste was extruded at a single ram velocity over a 100 mm ram displacement at a temperature of 21 ± 2 °C and room humidity of 35 ± 3%. Readings of extrusion force and ram displacement were logged on a PC. The mean extrusion pressure was evaluated using $P_{ex} = 4F/\pi D_{ram}^2$, where F is the force on the ram and D_{ram} is the ram diameter.

2.2.2. Single- and multi-holed die studies

Stainless steel dies with different numbers of holes (N) were fabricated, all with $D = 1$ mm and $L = 2$ mm, as shown in Fig. 3 and summarised in Table 3.

Extrusion experiments were performed at a wide range of ram velocities, from 0.025 to 10 mm s^{-1}. The protocol was similar to that described above. In order to study the liquid distribution within the barrel and the extruding paste, three samples of extrudate were collected during an extrusion run. Each sample consisted of the extrudate produced over a ram displacement interval of 10 mm. The first was collected at the start, when extrudate first emerged from the die land. The second and third samples were collected at ram displacements of 45–55 and 90–100 mm (*i.e.* middle and end of run), respectively. The plug of paste recovered from the barrel after the run was about 64 mm long and 25 mm in diameter (*i.e.* D_0). It was cut into three sections, which were labelled as bottom (in contact with the die), middle, and top (in contact with the ram), of approximate thicknesses 20, 20 and 24 mm, respectively. The extrudate samples and plug slices were dried as described above to yield the water content.

After some of the tests, about 50 g of fresh extrudate was subsequently spheronised using a Caleva spheronisor 120 (Caleva Process Solutions Ltd., Dorset, UK), fitted with a 120 mm diameter cross-hatched plate rotating at 1600 rpm for 30 s. Around 45 g of the MCC/water pellets obtained was then dried as described above.

2.3. Pellet characterisation

Pellet size and shape were measured using a Morphologi G2 automated microscopy system (Malvern Instruments Ltd., Worcestershire, UK), using a 1× magnification lens. Large agglomerates were occasionally formed during spheronisation and were also seen amongst the pellets recovered from the oven after drying. Pellet samples were initially sieved through a 2.8 mm mesh followed by a 355 μm mesh, after which a spinning riffler (Microscal Ltd., London, UK) was used to select 400 pellets for testing. Pellet size is presented as circle equivalent diameter, d_{CE}, where d_{CE} is the diameter of a circle with projected area equal to that of the pellet. The shape parameter reported here is the aspect ratio, AR, defined as L_{min}/L_{max}, where L_{max} and L_{min} are the largest dimension on a 2-dimensional projection of a particle and the dimension 90° normal to it, respectively. This differs from the parameters employed by workers such as Chopra et al. (2002), who report AR as L_{max}/L_{min}.

3. Results and discussion

MCC pellets, which are produced via E–S using single and multi-holed dies, were analysed to characterise their size and shape distributions.

3.1. Pellets from multi-holed die E–S

3.1.1. Extrusion velocity of 46 mm s^{-1}

Spheronisation was performed on extrudates obtained from extrusions using single- and multi-holed dies at an extrusion

velocity of 46 mm s^{-1}, corresponding to ram velocities of 0.073, 0.44, 2.40 and 10 mm s^{-1} for N = 1, 6, 33 and 137 dies, respectively. The recorded ram force profiles were steady. This extrusion velocity lies below the range of V_N values anticipated to occur in the pilot plant screen extruder (see Table 2), but higher velocities were not achievable with N = 137 with the strain frame. The ram velocities do, however, lie near the estimated values of V^*, indicating that the conditions for onset of LPM during the conveying of material towards the nip could be investigated. The water content of the plug recovered from the barrel was measured as about 55.5 wt%, which was close to that of the original paste (~55.8 wt%). This confirmed that LPM was not occurring in these tests. The extrudates all had smooth surfaces and could be successfully spheronised to yield spherical pellets.

Examples of non-dimensionalised pellet size and shape distributions, obtained with N = 137, are presented in Fig. 4 alongside the distribution with N = 1. The pellet size is non-dimensionalised with respect to die diameter (D = 1 mm). The distributions for other multi-holed die pellets are not presented, as they showed similar features. The mean d_{CE}/D and aspect ratios are summarised in Table 4.

The pellet size distribution data exhibit a long tail above the mode which suggests that they are log-normally distributed. The log-normal distribution model has two parameters, namely the arithmetic mean and the standard deviation of ln(d_{CE}/D) (Wu et al., 2005). Fig. 4(a) shows reasonable agreement between the model and the N = 137 die pellet data: the number distribution curve is unimodal with a modal d_{CE}/D value of 1.25. The shape distribution plot (Fig. 4(b)) indicates that most pellets in the size range of 0.9–1.7 mm have an AR value ≥ 0.80, which is taken to be a threshold for acceptable shape (Chopra et al., 2002). Some larger pellets (agglomerates) have smaller aspect ratios. The log-normal distribution parameters obtained for each die configuration are summarised in Table 4. The coefficient of determination, R^2, was used to quantify the goodness of fit. The data indicate a number mean d_{CE} of 1.3 mm with acceptable shape since their mean AR values are larger than 0.8. The means and standard deviations all lie within the bounds of experimental error, while the R^2 values are similar, indicating that the log-normal distribution provides a reasonable description of the data. The results show that multi-holed die extrusion is able to generate extrudates that produce pellets of equivalent quality to those obtained using single-holed dies.

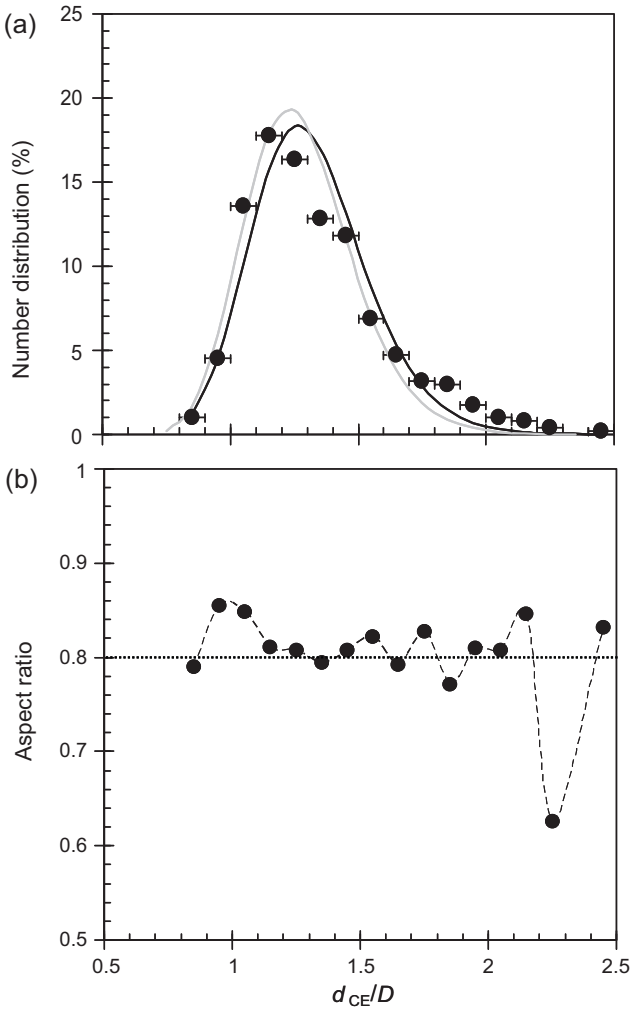

Fig. 4. Pellet size and shape distributions obtained using N = 137 die with V = 46 mm s^{-1}. (a) Number distributions: data points for N = 137 die, range bars indicate sizing bin width. Loci: solid line, log-normal distribution fitted to pellets from N = 137 die; grey line, log-normal distribution for N = 1 die (data not plotted). (b) Aspect ratio distribution for N = 137: horizontal dotted line shows the threshold value for acceptable quality of 0.8.

3.1.2. Extrusion velocity of 18 mm s^{-1}

Dies with N = 1, 6, 33 and 137 were used for extrusion at V = 18 mm s^{-1}, and the extrudates were subsequently spheronised to produce pellets. This velocity is discussed as LPM was evident during the single-holed die test (discussed in Section 3.3), where P_{ex} increased significantly over time. In contrast, no LPM was observed during the multi-holed die extrusion tests at this velocity.

No pellets smaller than 355 μm were formed. For most batches of pellets, less than 1% by mass of the pellets were larger than 2.8 mm. For the single-holed die extrusion at V = 18 mm s^{-1}, however, about 10% of the pellets were larger than 2.8 mm and these oversized pellets were removed from the sample by sieving. Fig. 5 shows examples of pellet size and shape distributions, and the associated log-normal distribution parameters are presented in Table 5. The figure shows that pellets produced via single-holed die extrusion at this relatively low velocity have a broader size distribution than those generated using the 137-holed die. The latter yielded pellets with a much narrower size range, with number mean d_{CE}/D = 1.33: other multi-holed dies gave similar profiles. A small number of pellets with d_{CE} < 0.65 mm and some agglomerates larger than 3 mm were again observed with multi-holed dies. A large number of agglomerates were obtained following single-holed die extrusion, which is consistent with the large modal value

Table 4
Pellet size and shape distribution parameters (mean ± standard deviation) for pellets obtained with V = 46 mm s^{-1}.

N	Number mean d_{CE}/D	Number mean AR	Log-normal distribution parameters		
			Geometric mean of d_{CE}/D	Standard deviation of ln(d_{CE}/D)	R^2
1	1.27 ± 0.26	0.81 ± 0.09	1.26	0.17	0.80
6	1.30 ± 0.24	0.81 ± 0.09	1.28	0.17	0.91
33	1.29 ± 0.25	0.81 ± 0.09	1.27	0.18	0.87
137	1.33 ± 0.28	0.81 ± 0.10	1.30	0.17	0.92

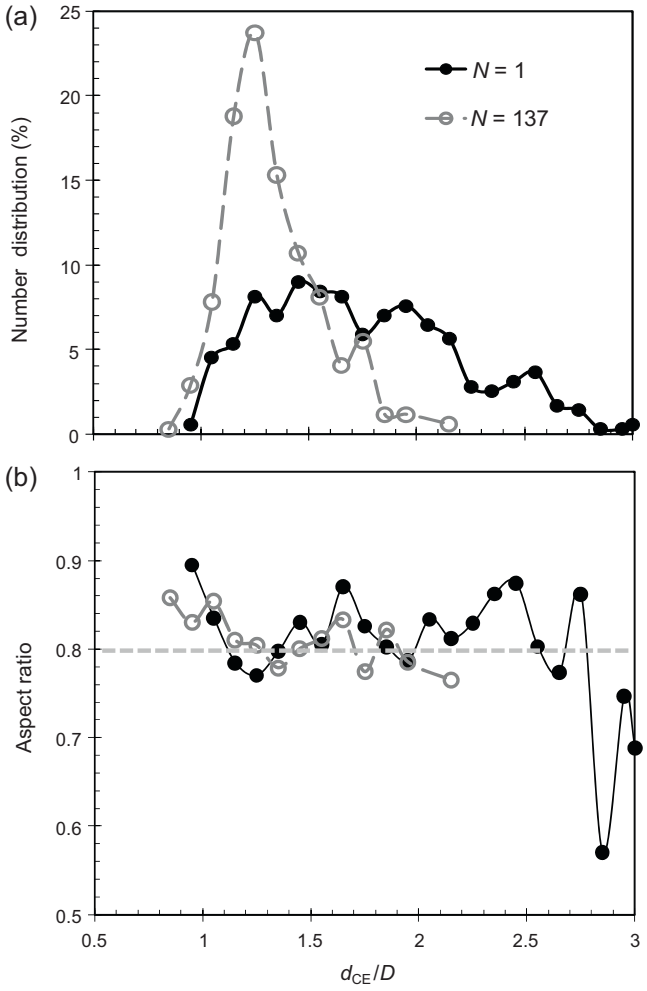

Fig. 5. Pellet (a) size number distributions; (b) aspect ratio distributions obtained for $V = 18\ mm\ s^{-1}$ using $N = 1$ (solid symbols) and 137 (open symbol) dies. The horizontal dotted line in (b) shows the *AR* quality threshold.

in Fig. 5 and high mean d_{CE}/D in Table 5. Fig. 5(b) indicates that most pellets are of an acceptable shape with mean *AR* larger than 0.8.

The observations show that LPM was not occurring with multi-holed die extrusions at $V = 18\ mm\ s^{-1}$ and good quality pellets with a relatively narrow size distribution were subsequently produced. For a given extrusion velocity, multi-holed die systems will have to operate at proportionally higher ram velocities than single-holed die tests. Consequently, the multi-holed die extrusion timescale is shorter than that of the single-holed die. A benefit of this is that multi-holed dies can mitigate LPM at low extrusion velocities, where a single-holed die system may incur severe LPM. LPM causes water maldistribution in the extrudates, and results in pellets with a broad size distribution and poor shape characteristics.

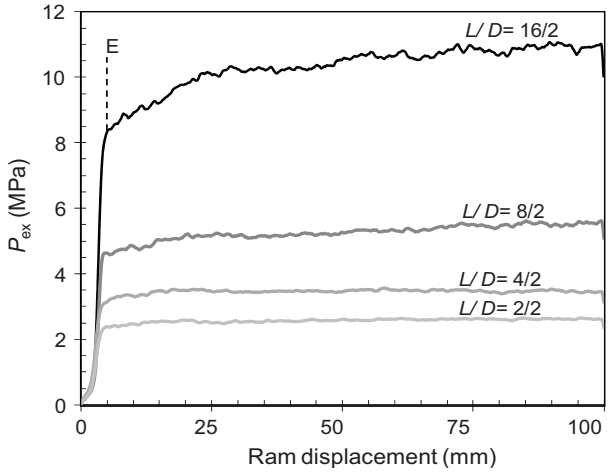

Fig. 6. Examples of extrusion pressure profiles. 45 wt% MCC/water paste, $V_{ram} = 2\ mm\ s^{-1}$ ($V = 310\ mm\ s^{-1}$), $D_0 = 25$ mm, $D = 2$ mm, $N = 1$ for various die lengths, *L*. The initial rapid increase in P_{ex}, marked E, represents the onset of extrusion.

3.2. Extrusion in the absence of LPM

3.2.1. Characterisation of 45 wt% MCC/water paste using single-holed dies

Ram extrusion tests of the 45 wt% MCC/water paste were performed using three sets of single-holed square-entry dies with different die diameters (*i.e.* $D = 1$, 2 and 3 mm, refer to Fig. 2 for geometry). Some examples of extrusion profiles are shown in Fig. 6. The initial rapid increase in P_{ex} (marked as E) is due to the paste entering the die land. In the following discussion, the extrusion pressure (P_{ex}) refers to the mean extrusion pressure, which was taken as the average of the experimental values from a ram displacement of about 5–100 mm. P_{ex} was used to generate Bagley-type plots (Steffe, 1996). Fig. 7 shows a series of the plots obtained at different extrusion velocities using 2 mm diameter dies. The pressure drop in the die entry region (P_1 term in Eq. (4)), and thus the bulk yield stress term, σ_y, can be estimated from the intercepts on the P_{ex}-axis. The linear Bagley-type plots indicate that the wall shear stress is constant for a given *V* and independent of the local pressure: paste-wall Coulombic friction is therefore not important, and a single value of the wall shear stress, τ_w, can be extracted from the gradient of each plot.

Fig. 8(a) shows a plot of σ_y against *V*: the data indicate a negligible velocity dependency for all three die diameters, *i.e.* the paste is strongly pseudo-plastic and its bulk yield behaviour can be described by a single parameter, $\sigma_y = 0.28 \pm 0.10$ MPa. Fig. 8(b) shows the corresponding plot of the wall shear stress, τ_w, against *V*. The trend in the data suggests a power law or Herschel–Bulkley relationship between τ_w and *V*. The data sets for the different diameters lie close to each other, particularly for the 1 and 3 mm diameter dies, with the 2 mm die data showing a slightly different trend. There is no systematic variation with die diameter. This supports a wall slip model, which assumes that the paste moves in plug flow and shearing only takes place within a thin layer of material

Table 5
Pellet size and shape distribution parameters (mean ± standard deviation) for pellets obtained with $V = 18\ mm\ s^{-1}$.

N	Number mean d_{CE}/D	Number mean *AR*	Log-normal distribution parameters		
			Geometric mean of d_{CE}/D	Standard deviation of $\ln(d_{CE}/D)$	R^2
1	1.74 ± 0.45	0.82 ± 0.10	1.69	0.26	0.85
6	1.46 ± 0.35	0.83 ± 0.09	1.43	0.22	0.84
33	1.46 ± 0.32	0.82 ± 0.10	1.43	0.21	0.87
137	1.33 ± 0.22	0.81 ± 0.10	1.31	0.16	0.91

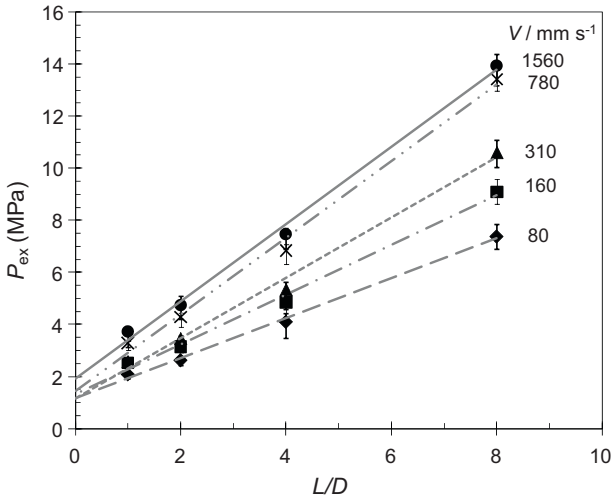

Fig. 7. Bagley-type plots for extrusion of 45 wt% MCC/water paste using $D = 2$ mm single-holed dies. $D_0 = 25$ mm. Extrusion velocities indicated. Error bars represent the range in data observed in experiments.

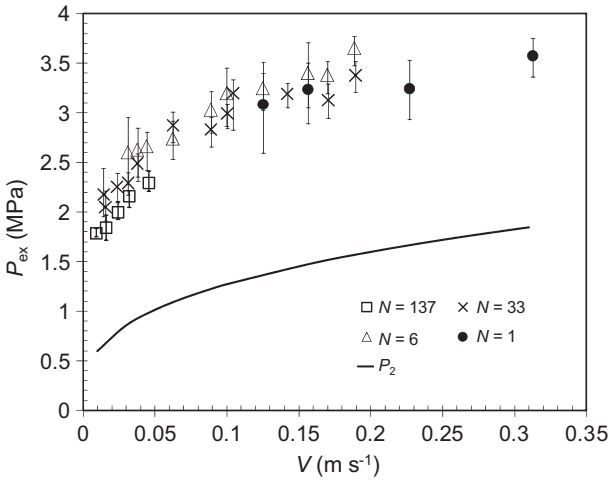

Fig. 9. Effect of extrusion velocity on P_{ex} for single and multi-holed dies. Points represent experimental data. The error bars represent the experimental range. The solid locus shows the P_2 values estimated using Eq. (7).

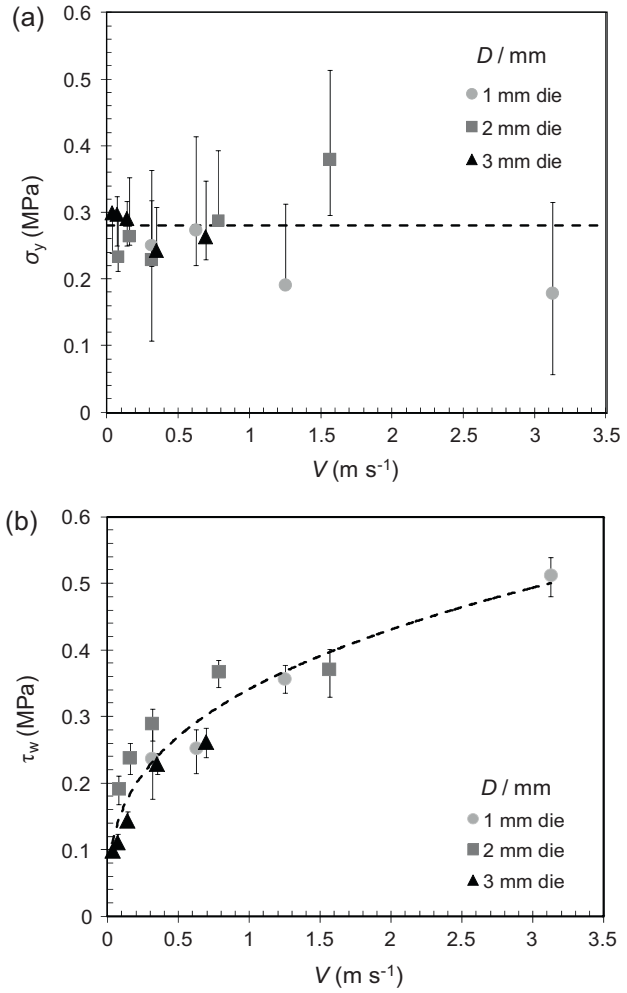

Fig. 8. 45 wt% MCC/water paste characterisation. Plots of (a) bulk yield stress and (b) wall shear stress at various extrusion velocities for $D = 1$, 2 and 3 mm single-holed dies. Error bars indicate the minimum and maximum values extracted from experimental variations. Dashed line in (a) indicates a σ_y value of 0.28 MPa. Dashed locus in (b) represents the power law curve fit to the experimental data.

near the die wall. Compared to the bulk yielding behaviour, strain rate (velocity) effects are significant. The data could also be plotted in the form of flow curves, *i.e.* τ_w against apparent shear strain rate ($8V/D$). These gave widely separated data sets and there was no systematic variation with D, supporting the wall slip description. The apparent shear strain rates corresponding to the data sets in Fig. 8 are: $D = 1$ mm, 2500–25 000 s^{-1}; $D = 2$ mm, 310–6250 s^{-1}; $D = 3$ mm, 93–1850 s^{-1}. These cover the range of shear strain rates estimated for the screen holes in Table 2, and the higher end of the range estimated for the nip gap.

The plots in Fig. 8 show that neither σ_y nor τ_w is dependent on the die diameter. The limiting wall shear stress, τ_0, *i.e.* the wall shear stress when $V = 0$ (see Eq. (5)), could not be accessed experimentally using the $D = 1$ mm set of dies as LPM was observed for the longest die ($L = 12$ mm) at extrusion velocities lower than 310 mm s^{-1} (corresponding to $V_{ram} = 0.5$ mm s^{-1}); however, larger dies (*e.g.* $D = 3$ mm) could be used at lower V since LPM was not evident with these.

Experimental data obtained from the 1, 2 and 3 mm diameter die sets were fitted to Eq. (5) and gave the parameters $\sigma_y = 0.28$ MPa, $\tau_0 = 0$ MPa, $\beta = 0.34$ MPa $(m\,s^{-1})^{-0.33}$, $n = 0.33$. With these parameters, Eq. (6) then becomes (in dimensional form)

$$P_{ex,BB}\ (\text{MPa}) = P_1 + P_2 = 0.28 \ln\left(\frac{A_0}{NA}\right) + 4(0.34V^{0.33})\frac{L}{D} \qquad (7)$$

where $P_{ex,BB}$ is the extrusion pressure given by the Benbow et al. model and V is in m s^{-1}.

3.2.2. Multi-holed die extrusion

Multi-holed extrusion tests were performed using dies with $N = 1$, 6, 33 and 137, all with $L/D = 2/1$ mm/mm: the extrusion profiles showed similar features to those presented in Fig. 6. The reported extrusion pressure (P_{ex}) is the average of the experimental values between ram displacements of 25 and 100 mm. The data discussed in this section were obtained from extrusion tests that did not exhibit LPM.

3.2.2.1. Comparison with Benbow et al. model prediction. The multi-holed die extrusion pressures are compared with the Benbow et al. model. Plots of experimental extrusion pressure (P_{ex}) against extrusion velocity (V) are shown in Fig. 9. The solid locus in the figure is the P_2 contribution estimated using Eq. (7), which should be common to all dies ($L/D = 2$) at a given value of V (assuming an even

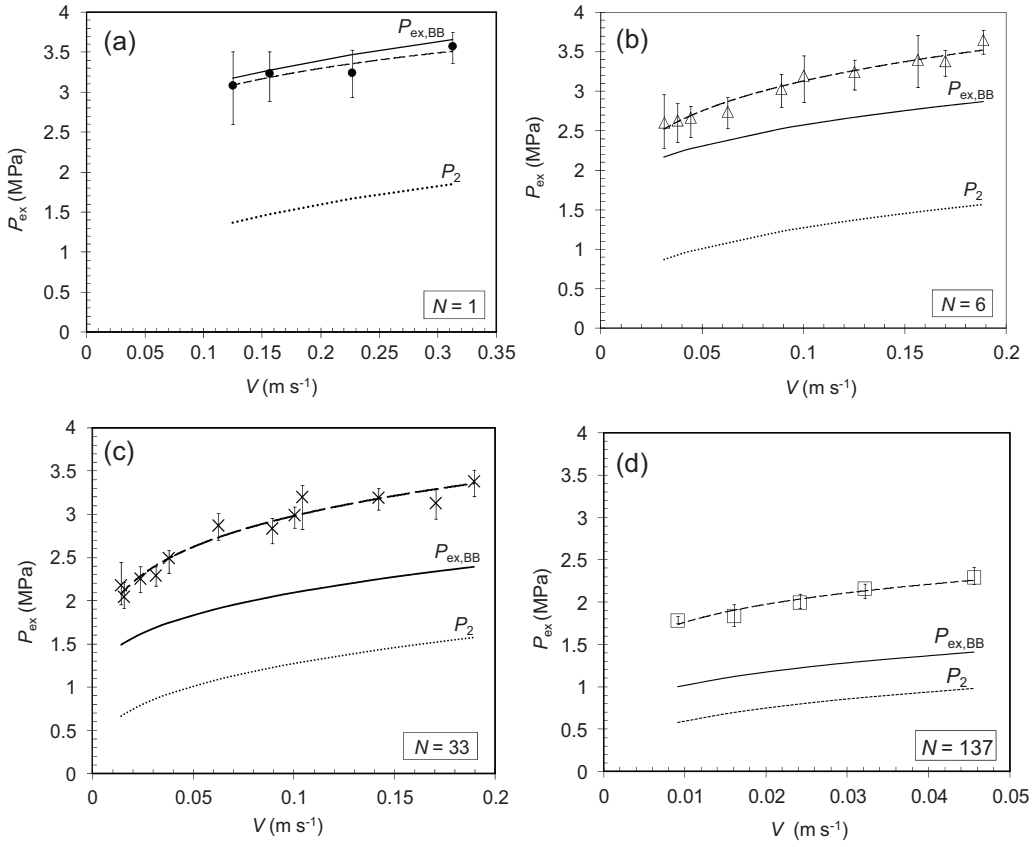

Fig. 10. Plots of extrusion pressure (P_{ex}) against extrusion velocity (V) for different dies, all D = 1 mm and L = 2 mm. Points represent experimental data. The error bars represent the experimental data range observed in experiments. Dashed loci are power law curve fits to the experimental data. Solid and dotted lines represent $P_{ex,BB}$ and P_2, respectively, both estimated using Eq. (7).

distribution of paste as it flows towards the die face). The experimental data show that P_{ex} increases as V increases for a given die, as expected. The data from the different dies lie close to each other. The pressure drop across the die entry region (P_1) and the pressure drop along the die land (P_2) make almost equal contributions to the overall pressure drop (P_{ex}). The dependence of extrusion pressure on the number of die holes is relatively weak, which represents a deviation from Eq. (7). The P_2 term appears to be the dominant contributor to the velocity dependency in P_{ex}. This is consistent with the characterisation parameters, where P_2 is a function of V, while P_1 (*i.e.* σ_y) is not.

In Fig. 10, the experimental data are compared with the Eq. (7) predictions. It should be noted that the V axes have different scales, because extrusion tests using different dies had to be performed over different V ranges. For all of the tests, the highest V_{ram} was limited to 10 mm s^{-1} by the strain frame. The lowest ram velocity was set as that which avoided significant LPM. In all cases, $P_2 < 1/2P_{ex}$.

The Benbow et al. model provides a good prediction of the extrusion pressures for the single-holed die, which is expected as the characterisation parameters were generated by analysing data from single-holed die tests. In comparison, the model consistently underestimates the overall extrusion pressures for the multi-holed dies, although it provides a better estimate for the 6-holed die than for the 33-holed and 137-holed dies. The differences between P_{ex} and $P_{ex,BB}$ are estimated in terms of the percentage of the pressure drop in the die entry region ($P_{ex} - P_2$): the average differences for N = 6, 33 and 137 are 28%, 49% and 65%, respectively. Thus the discrepancy increases with increasing N.

3.2.2.2. Experimental P_1 vs estimated P_1. The Benbow et al. model (Eq. (7)) describes the flow in the die entry region as approximating homogeneous deformation. It predicts that P_1, and consequently $P_{ex,BB}$, should decrease for a given set of process conditions (*i.e.* a given paste formulation and extrusion velocity) if there are more holes in the die. The major uncertainty lies in the estimation of the contribution from redundant work. Noting that the units of pressure are work per unit volume, the contribution from redundant work was estimated from the following:

$$P_{redundant} \cong P_{ex} - P_{ex,BB} \quad (8)$$

where $P_{ex,BB}$ is the Benbow et al. estimate (Eq. (7)), which is treated as accounting for the ideal work done in the die entry region and along the die land wall. Plots of $P_{redundant}$ against V are presented in Fig. 11, which show a weak dependence of $P_{redundant}$ on the extensional strain rate (related to V/D) for a given die plate. Compared to 33 and 137-holed dies, the 6-holed die produces slightly smaller values of $P_{redundant}$; nevertheless, there is no systematic variation with N. These data confirm that redundant work provides a significant contribution to the extrusion pressure, and more accurate predictions require further, detailed simulation of these highly non-axisymmetric flow fields.

3.3. Investigation of LPM in multi-holed die extrusion

3.3.1. Single- vs multi-holed dies

LPM is usually evident in single-holed die extrusion at a relatively low extrusion velocity. If LPM is related to the total time for which the paste is subject to high pressure (as described by Wroth and Houlsby, 1984, and applied to several pastes by Martin

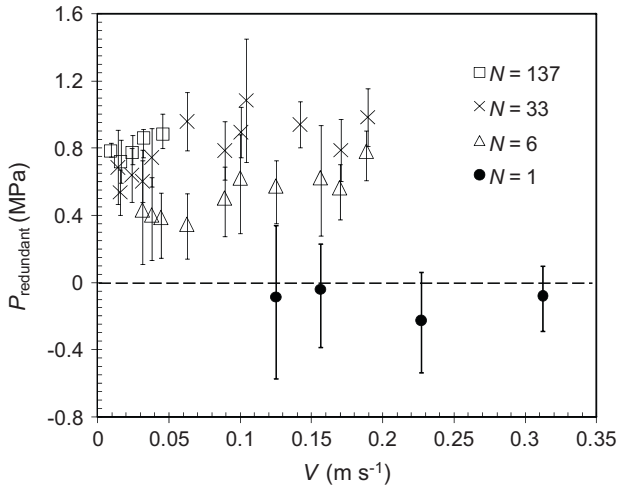

Fig. 11. Effect of extrusion velocity on estimated redundant work per unit volume in the die entry region. 45 wt% MCC/water paste, D_0 = 25 mm, single and multi-holed dies, D = 1 mm and L = 2 mm. The horizontal dashed line shows zero value for redundant work per unit volume.

et al., 2006), multi-holed die extrusion at the same V would not promote LPM as the test would run at a proportionally higher ram velocity (*i.e.* with a shorter processing time). In order to establish the impact of large hole area fractions on LPM, extrusion profiles, together with the extrudate and barrel plug liquid contents, were investigated for single, 6, 33 and 137-holed dies (all with D = 1 mm and L = 2 mm) at an extrusion velocity of 16 mm s^{-1} (corresponding to ram velocities of 0.025, 0.15, 0.84 and 3.5 mm s^{-1}, respectively). Figs. 12 and 13 show the associated P_{ex} and liquid content profiles. Due to the variability in experimental conditions, such as temperature and humidity, the liquid content of the paste used for each extrusion test can deviate from that of the initial bulk paste, and may differ between runs. The following discussion of the liquid content data in Fig. 13 is therefore based on relative liquid distributions within a given sample.

The extrusion pressure profiles in Fig. 12 differ noticeably in data scatter. Russell et al. (2004) used the coefficient of variation (CoV) of P_{ex} profiles to monitor the homogeneity of clay-based detergent pastes. There, poorly mixed or inhomogeneous pastes gave larger CoV values. A similar approach was applied here, where the CoV was calculated as the ratio of the standard deviation in P_{ex} to the P_{ex} value at a ram displacement of 25 mm (*i.e.* D_0). The standard deviation was calculated from the difference between P_{ex} and a trendline based on a central moving average across 62 displacement points: the trendlines are plotted in Fig. 12. $P_{ex,\,25\,mm}$ was considered as a suitable reference since at this point extrudate had always emerged from the die and LPM effects were not well-developed. The CoV values are reported alongside the extrusion operation time, *i.e.* the time taken for the test, in Table 6.

A noticeable increase in P_{ex} over time is evident with the single-holed die in Fig. 12(a), which suggests that LPM is occurring. The P_{ex} data also show noticeable fluctuations, which are attributed to uneven water distribution in the barrel paste; the associated CoV in Table 6 is larger than those of the multi-holed dies. The occurrence of LPM is confirmed by the water distribution data. The extrudate for the single-holed die in Fig. 13(a) exhibits a steady decrease in water content, changing by ~5 wt% over the course of the run, while

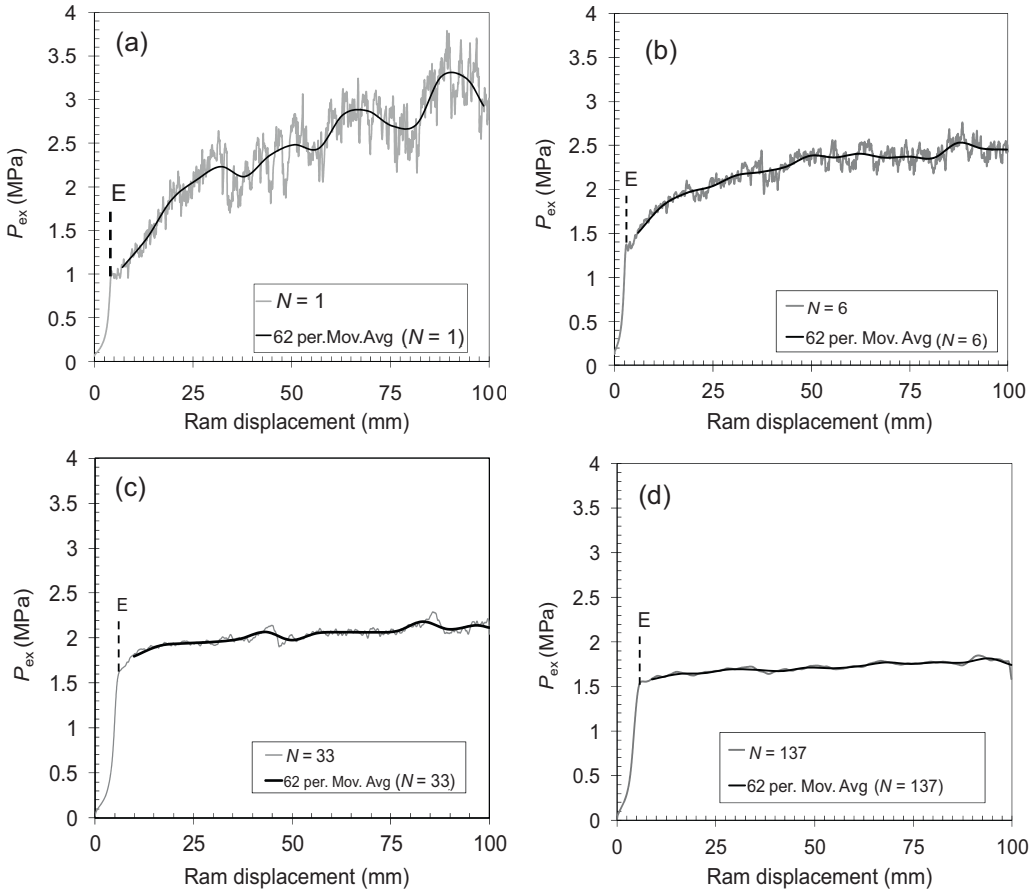

Fig. 12. Ram extrusion pressure–displacement profiles for 45 wt% MCC/water pastes for an extrusion velocity of 16 mm s^{-1}: (a) single-holed die; (b) 6-holed die; (c) 33-holed die; and (d) 137-holed die. D_0 = 25 mm, square-entry dies, D = 1 mm and L = 2 mm. The initial rapid increase in P_{ex}, marked E, represents the onset of extrusion.

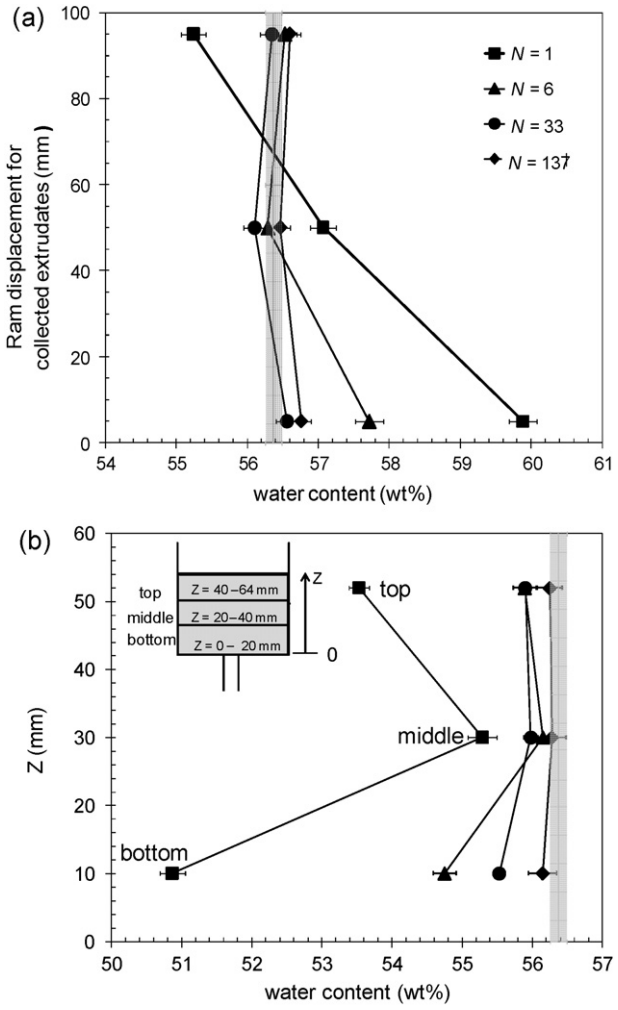

Fig. 13. Liquid content profiles for (a) extrudates and (b) barrel plugs associated with Fig. 12. The grey bands represent the measured initial bulk paste water content. Error bars show uncertainty in the experimental measurements.

Table 6
CoV values for extrusion pressure profiles in Fig. 12 (extrusion velocity 16 mm s^{-1}).

N	Ram velocity (mm s^{-1})	CoV	Processing time (s)
1	0.025	0.11	4000
6	0.15	0.04	667
33	0.84	0.02	119
137	3.5	0.01	29

the water distribution within the barrel plug in Fig. 13(b) varies by about 4 wt% between the middle and the bottom slice. Similar observations were reported by Rough et al. (2002). Fig. 13 also shows relatively uniform water distributions in the extrudates and barrel plugs from each of the multi-holed die tests, which is consistent with the steady extrusion pressure profiles in Fig. 12(b–d).

In summary, for an extrusion velocity of 16 mm s^{-1}, the single-holed die extrusion experienced severe LPM and produced extrudates with non-uniform water contents, whereas the multi-holed dies, *i.e.* N = 6, 33 and 137, gave steady extrusion pressures and relatively homogeneous water distributions within the paste extrudates and barrel plugs. This indicates that the multi-holed dies are able to mitigate LPM which may occur during single-holed die tests at low extrusion velocities.

The threshold velocities for LPM with multi-holed dies are significantly lower than the V_N values estimated in the pilot plant extruder (Section 1.1, Table 2), but can overlap the range estimated for V^*, *i.e.* in the approach to the screen, particularly for single-holed dies.

3.3.2. Threshold velocity for LPM

Figs. 12 and 13 show that there is a difference in the velocity at which the onset of LPM is observed between the single and multi-holed dies. There are a number of possible explanations for this difference and these are explored in this section. Pastes are granular materials and the stress imposed on a paste to force it through a die is shared by the solids matrix and liquid binder. The latter component, termed the pore pressure in soil mechanics, can cause the liquid phase to move relative to the solids and this will be exacerbated when the solids move slowly relative to the (associated) liquid drainage rate. LPM in pastes has been studied by several workers for both ram extrusion and squeeze flow geometries (*e.g.* Mascia et al., 2006; Kaci et al., 2011), and the explanations and models proposed to explain LPM can be classified in terms of three mechanisms:

I. *Consolidation in billet*. Paste approaching a die plate is subjected to the loading required to extrude the material and this can cause consolidation and hence drainage. Martin et al. (2006) applied the criterion for the onset of LPM in ram extrusion developed by Wroth and Houlsby (1984) from soil mechanics principles to several data sets reporting LPM, including one MCC/water paste. Many of the reported studies fitted this criterion. The controlling parameters in this case are the duration of extrusion (related to the ram velocity, V_{ram}), pore pressure in the liquid phase, and the permeability of the paste.
II. *Dilatancy and suction*. When a granular material, such as a soil, is strained in extension it can be forced to increase in volume in order to flow. Since the volume of the particulate phase is fixed, the change in volume is either matched by an inflow of liquid or vapour (cavitation). Both create suction forces in the liquid phase, drawing liquid into the die entry region where extensional deformation occurs. Mascia et al. (2006) showed that the onset of LPM in MCC/water pastes undergoing ram extrusion and squeeze flow could be related to extensional strain rates (and thus die entry suction effects). Modelling of suction effects requires detailed simulation of pore pressures in a deforming matrix, as reported by Patel et al. (2007). Controlling parameters include the extensional strain (for a homogeneous deformation, related to $\ln\{A_0/NA\}$) and shear strain rate (related to V/D), the material yield behaviour, paste permeability, *etc.*
III. *Die land drainage*. Yaras et al. (1994) observed a threshold for LPM in the ram extrusion of highly filled suspensions simulating rocket propellants. They related the threshold to a competition between the superficial velocity of liquid draining through the die land due to the imposed pressure drop, and the velocity of the solids along the die land due to the same pressure drop. They reported good agreement between their prediction and observed values, although their model appears to let the energy dissipated against wall friction be simultaneously dissipated against the pore pressure in the paste matrix. Controlling parameters are the extrusion pressure P_{ex}, V, L and paste permeability.

All three mechanisms predict that LPM will be encountered at lower extrusion velocities, where the rate of liquid movement becomes comparable with the rate of convection of material through the die. Determining which, if any, mechanism is controlling is hampered by the difficulty in measuring pore pressures and small changes in voidage in extruding pastes. Assessing the relative permeability of the solids matrix is also challenging.

For a given V, with a larger number of die holes, the paste experiences shorter processing times in the barrel as well as lower

Table 7
Summary of LPM thresholds: $D = 1$ mm, $L = 2$ mm.

N	Range of ram velocities tested ($mm\,s^{-1}$)	Number of velocities tested	Lowest ram velocity without promoting LPM ($mm\,s^{-1}$)	Threshold ram velocity ($mm\,s^{-1}$)	Threshold extrusion velocity ($mm\,s^{-1}$)	Processing time (s)	Extrusion pressure[a] (MPa)	Plug water content[b] (wt%)	Estimated $\dot{\varepsilon}\lambda$ ($mm\,s^{-1}$)
1	0.025–0.50	11	0.070	0.05	31	2000	2.4	54.2	0.32
6	0.080–4.0	20	0.15	0.08	8	1250	2.0	54.5	0.37
33	0.025–10	13	0.60	0.15	3	667	2.3	54.5	0.44
137	0.025–10	13	0.45	0.25	1	400	2.2	54.1	0.38

[a] The pressure stated is that obtained at a ram displacement of 25 mm ($P_{ex,\,25\,mm}$).
[b] The initial paste water content was about 56.1 wt%.

extensional strain rates. As a consequence, LPM may commence at different ram velocities for different N. It was decided to investigate both single-holed and multi-holed die extrusion further so that the threshold ram velocities where LPM becomes significant for each die could be identified and insights given into the likely controlling mechanism.

A steady increase in extrusion pressure over the course of an extrusion test is indicative of LPM, which can be confirmed by measurements of extrudate and barrel plug liquid contents. Since LPM by mechanism I is strongly affected by processing time and the time spent in the barrel (see Martin et al., 2006), all the extrusion experiments are reported here in terms of ram, rather than extrusion, velocity. Series of tests established a threshold ram velocity, $V_{ram,LPM}$, for each die, below which substantial LPM was observed. Typically four tests were performed, spanning the range of velocities over which LPM became evident. The threshold value reported is the experimental value nearest the midpoint of the transition. The threshold velocities, together with other pertinent information, are summarised in Table 7. $P_{ex,\,25\,mm}$ is about 2.2 MPa for all tests. All plugs contain ~54 wt% of water, which is lower than the initial paste water content.

It can be seen that $V_{ram,LPM}$ increases as the number of die holes increases, whereas the corresponding extrusion velocity decreases. Since P_{ex} and L are similar but $V_{ram,LPM}$ varies with N, the data indicate that die land drainage (mechanism III) is not the controlling mechanism. Similarly, the variation in $V_{ram,LPM}$ with N does not support consolidation in the billet (mechanism I) as controlling LPM in this case: the processing times vary noticeably with N. Positive evidence supporting mechanism II is provided by estimating the extensional strain rate at the die entry region, $\dot{\varepsilon}$, as:

$$\dot{\varepsilon} \propto \frac{\text{extensional strain}}{\text{timescale}} \approx \frac{\ln(A_0/NA)}{\lambda/V_{ram,LPM}} = \frac{V_{ram,LPM}}{\lambda} \times \ln\left(\frac{A_0}{NA}\right) \quad (9)$$

A characteristic length scale, λ, remains to be defined in estimating $\dot{\varepsilon}$ via Eq. (9). Assuming that this length scale is common to all dies used in these tests, the values in Table 7 are similar and can be considered to show reasonable agreement, particularly given the degree of approximation involved in the estimate. These results therefore appear to support the findings of Mascia et al. (2006). Eq. (9) involves several approximations, particularly in terms of λ, so confidence intervals are not estimated: this is the subject of ongoing work.

A further observation particular to multi-holed die extrusion was the blockage of die holes for velocities lower than or equal to the threshold velocity for LPM. For example, with the 6-holed die, four holes blocked over the duration of the extrusion test at a ram velocity of 0.08 $mm\,s^{-1}$. Over the series of tests it was noticeable that where one or several holes became blocked during the experiment, the central hole was always the first (sometimes the only) hole to become blocked. This suggests that an uneven water distribution was developed across the die face during the extrusion and the central part of the barrel paste was drier than the outer region. The holes were blocked by the relatively dry (and stiffer) paste. Unfortunately, the resolution of the sectioning and weighing of the barrel plug was too coarse to determine the radial paste water distributions over the cross-section of the barrel plug. When extruding through the 33-holed die at ram velocities < 0.15 $mm\,s^{-1}$, more than two thirds of the holes became blocked, and when extruding at 0.25 $mm\,s^{-1}$ through the 137-holed die, only 11 holes were still active at the end of the test.

4. Conclusions

The use of square-entry, multi-holed dies to generate extrudates for subsequent spheronisation was investigated as an alternative to

extrusion using single-holed dies. The pellets generated by multi-holed extrusion–spheronisation were comparable in size and shape to those obtained using single-holed dies, with the advantage that the multi-holed systems could be used at lower extrusion velocities before encountering problems caused by liquid phase migration (LPM), particularly observed in single-holed dies. A simple model of screen extrusion operation indicated that the characteristic velocities in screen extrusion devices belonged to two groups, namely high velocities and shear strain rates associated with flow through the screen holes, and low velocities on the approach to the blade and nip region. LPM was therefore more likely to arise in the latter region and cause problems as harder material passed through the screen.

The rheology of the MCC/water paste used in these studies was characterised using the Benbow–Bridgwater approach and the extrusion pressures for the multi-holed dies compared with the model proposed by Benbow et al. (1991). The latter was found to underpredict the observed extrusion pressures, which was attributed to the model not accounting for redundant work accurately. The redundant work component was quantified and found to depend more strongly on the number of die holes than extrusion velocity. Further study of this aspect requires detailed simulation and lies outside the scope of this paper.

Comparison of the operating conditions – primarily ram velocity – governing the onset of LPM for dies with 1–137 holes indicated that drainage in the die land and consolidation in the paste billet were not the governing mechanisms. A simple estimate of the extensional strain rate at the onset of LPM yielded similar values for all four die configurations studied, supporting the dilatancy and suction mechanism reported by Mascia et al. (2006). More accurate quantification of the critical extensional strain rate, and relating this to the flow in screen extrusion devices, is the subject of ongoing work.

Acknowledgements

Helpful discussions with Dr. David Scott on particle size distributions and an EPSRC Dorothy Hodgkin studentship for Min Zhang, supported by MSD, are gratefully acknowledged.

References

Baert, L., Down, G.R.B., 1994. A comparison of two methods of instrumenting a small-scale basket extruder. Int. J. Pharm. 107, 219–222.
Benbow, J.J., Bridgwater, J., 1993. Paste Flow and Extrusion. Clarendon Press, Oxford.
Benbow, J.J., Jazayeri, S.H., Bridgwater, J., 1991. The flow of pastes through dies of complicated geometry. Powder Technol. 65, 393–401.
Boutell, S., Newton, J.M., Bloor, J.R., Hayes, G., 2002. The influence of liquid binder on the liquid mobility and preparation of spherical granules by the process of extrusion/spheronization. Int. J. Pharm. 238, 61–76.
Chopra, R., Podczeck, F., Newton, J.M., Alderborn, G., 2002. The influence of pellet shape and film coating on the filling of pellets into hard shell capsules. Eur. J. Pharm. Biopharm. 53, 327–333.
Horrobin, D.J., Nedderman, R.M., 1998. Die entry pressure drops in paste extrusion. Chem. Eng. Sci. 53, 3215–3225.
Kaci, A., Ouari, N., Racineux, G., Chaouchea, M., 2011. Flow and blockage of highly concentrated granular suspensions in non-Newtonian fluid. Eur. J. Mech. B/Fluids 30, 129–134.
Martin, P.J., Wilson, D.I., Bonnett, P.E., 2006. Paste extrusion through non-axisymmetric geometries: insights gained by application of a liquid phase drainage criterion. Powder Technol. 168, 64–73.
Mascia, S., 2008. Rheology and processing of pharmaceutical pastes. Ph.D. Dissertation. University of Cambridge.
Mascia, S., Patel, M.J., Rough, S.L., Martin, P.J., Wilson, D.I., 2006. Liquid phase migration in the extrusion and squeezing of micro-crystalline cellulose pastes. Eur. J. Pharm. Sci. 29, 22–34.
Patel, M.J., Blackburn, S., Wilson, D.I., 2007. Modelling of paste flows subject to liquid phase maldistribution. Intl. J. Numer. Methods Eng. 72, 1157–1180.
Rahman, L., Rowe, P., Cheyne, A., Wilson, D.I., 2001. Ram extrusion of potato starch dough through multi-holed dies. Food Bioprod. Process. 80, 12–19.
Rough, S.L., Bridgwater, J., Wilson, D.I., 2000. Effects of liquid phase migration on extrusion of microcrystalline cellulose pastes. Int. J. Pharm. 204, 117–126.
Rough, S.L., Wilson, D.I., Bridgwater, J., 2002. A model describing liquid phase migration within an extruding microcrystalline cellulose paste. Chem. Eng. Res. Des. 80, 701–714.
Russell, B.D., Lasenby, J., Blackburn, S., Wilson, D.I., 2004. Monitoring structural aspects of pastes undergoing continuous extrusion using signal processing of pressure data. Chem. Eng. Res. Des. 82, 770–783.
Sinha, M.K., Deb, S., Das, R., Dixit, U.S., 2009. Theoretical and experimental investigations on the multi-hole extrusion process. Mater. Des. 30, 2386–2392.
Steffe, J.F., 1996. Rheological Methods in Food Process Engineering, 2nd edn. Freeman Press, East Lansing, MI, USA.
Wilson, D.I., Rough, S.L., 2007. Extrusion–spheronisation. In: Salman, A.D., Hounslow, M.J. (Eds.), Granulation. Elsevier, Amsterdam, pp. 189–210.
Wroth, C.P., Houlsby, G.T., 1984. Applications of soil mechanics theory to ceramics processing. In: Hench, L.L., Ulrich, D.R. (Eds.), Ultrastructure Processing of Ceramics Glasses and Composites. Wiley, New York, USA, pp. 448–463.
Wu, D.F., Zhou, J.C., Li, Y.D., 2005. Technical note: statistical analysis of pellet size variation in commercial catalysts. Part. Part. Syst. Charact. 22, 63–68.
Yaras, P., Kalyon, D.M., Yilmazer, U., 1994. Flow instabilities in capillary flow of concentrated suspensions. Rheol. Acta 33, 48–59.